catalysts

MDPI

Article

Tuning the Electronic Structure of CoO Nanowire Arrays by N-Doping for Efficient Hydrogen Evolution in Alkaline Solutions

Maoqi Cao *, Xiaofeng Li, Dingding Xiang, Dawang Wu, Sailan Sun, Hongjing Dai *, Jun Luo and Hongtao Zou *

School of Chemistry and Chemical Engineering, Qiannan Normal University for Nationalities, Duyun 558000, China; xiaofengli188@163.com (X.L.); xdd9822@163.com (D.X.); dawangwuqnsy@sina.com (D.W.); sunsailan1026@sina.com (S.S.); ejuluo@outlook.com (J.L.)

* Correspondence: caomaoqi@mail.ustc.edu.cn (M.C.); daixiaojing_520@163.com (H.D.); zouhongtao5580@sina.com (H.Z.)

Abstract: Electrochemical hydrogen evolution reactions (HER) have drawn tremendous interest for the scalable and sustainable conversion of renewable electricity to clear hydrogen fuel. However, the sluggish kinetics of the water dissociation step severely restricts the high production of hydrogen in alkaline media. Tuning the electronic structure by doping is an effective method to boost water dissociation in alkaline solutions. In this study, N-doped CoO nanowire arrays (N-CoO) were designed and prepared using a simple method. X-ray diffraction (XRD), element mappings and X-ray photoelectron spectroscopy (XPS) demonstrated that N was successfully incorporated into the lattice of CoO. The XPS of Co 2p and O 1s suggested that the electronic structure of CoO was obviously modulated after the incorporation of N, which improved the adsorption and activation of water molecules. The energy barriers obtained from the Arrhenius relationship of the current density at different temperatures indicated that the N-CoO nanowire arrays accelerated the water dissociation in the HER process. As a result, the N-CoO nanowire arrays showed an excellent performance of HER in alkaline condition. At a current density of 10 mA cm^{-1}, the N-CoO nanowire arrays needed only a 123 mV potential, which was much lower than that of CoO (285 mV). This simple design strategy provides some new inspiration to promote water dissociation for HER in alkaline solutions at the atomic level.

Keywords: CoO nanowires; N-doping; water dissociation; KOH; HER

Citation: Cao, M.; Li, X.; Xiang, D.; Wu, D.; Sun, S.; Dai, H.; Luo, J.; Zou, H. Tuning the Electronic Structure of CoO Nanowire Arrays by N-Doping for Efficient Hydrogen Evolution in Alkaline Solutions. *Catalysts* **2021**, *11*, 1237. https://doi.org/10.3390/catal11101237

Academic Editors: Angela Dibenedetto and Francesco Nocito

Received: 27 September 2021
Accepted: 12 October 2021
Published: 14 October 2021

1. Introduction

Due to severe environmental pollution as a result of the excessive consumption of traditional fossil fuels [1–4], it is desirable to explore clean and sustainable energy sources [5,6]. Hydrogen is of significant importance in sustainable energy systems and in the chemical industry; its advantages include its high energy density as well as being pollution-free [7–9]. Electrochemical hydrogen production with electric energy from renewable energy sources, such as wind energy and solar energy, has attracted some attention and has been applied in various hydrogen production technologies. However, the industrial application of water electrolysis is hampered by the performance and cost of HER catalysts. In water electrolysis, HER catalysts can be performed in basic, neutral or acidic solutions [10,11]. Currently, the best HER and oxygen evolution reaction catalysts are still Pt- and Ir/Ru-based materials [12,13], respectively. However, since most of the cost-effective oxygen evolution reaction catalysts on the counter electrode can only work under alkaline condition [14–16], developing highly efficient, robust and earth-abundant alkaline HER electrocatalysts is much more desirable [17–19].

Over the past few years, a lot of low-cost earth-abundant catalysts have been developed for HER, such as transition metal-based alloys [20–24], nitrides [25,26], carbides [27–29], phosphides [30–32], sulfides [33–35] and polymer catalysts [36–40]. Among

them, transition metal nitrides with excellent activity have attracted great attention. However, when compared in acid condition, their HER activities in alkaline media need to be further improved. Due to the sluggish kinetics of water dissociation in alkaline media, the reaction rates of transition metal nitrides for HER in alkaline solutions are about two to three orders of magnitude lower than in acidic solution [41,42]. Previous approaches to solving water dissociation in alkaline solutions focused on interface engineering. Some recent studies based on interface engineering have improved HER performance in alkaline solutions with the enhancement of water dissociation [31,43,44]. However, interface engineering relies on a well-designed interface, with features such as corners, edges and grain boundaries. In addition, the rare metal of Pt is often used to offer an optimal H adsorption energy in these approaches [45,46]. As such, developing new catalysts from a moderate method using earth-abundant elements with efficient water dissociation at atomic scale is highly desirable but challenging.

Tuning the electronic structure by heteroatom doping has been demonstrated to be an effective method to boost water dissociation in alkaline solutions [47–49]. CoO is a promising electrocatalyst for HER due to its abundance. However, its high water dissociation energy makes it unsuitable for HER in alkaline solutions [50]. Inspired by the reasons above, a simple and efficient strategy to solve the sluggish water dissociation kinetics of CoO electrocatalysts by N-doping was developed. X-ray diffraction (XRD), element mappings and X-ray photoelectron spectroscopy (XPS) demonstrated that the incorporation of N did not change the crystal structure of CoO. The XPS analysis of the Co 2p and O 1s of CoO and N-CoO proved that the adsorption and activation of water molecules was enhanced significantly after the incorporation of N, which was consistent with the energy barriers obtained from the Arrhenius relationship of the current density at different temperatures. As a result, the N-CoO nanowire arrays exhibited a very high activity, using only 123 mV to achieve the current density of 10 mA cm^{-2} and the low Tafel slope of 97 mV dec^{-1} in 1 M KOH.

2. Results

Figure 1 is the schematic illustration for the preparation of the CoO and N-CoO nanowire arrays. Briefly, the CoO and N-CoO nanowire arrays were obtained by annealing the precursor of the $Co_x(OH)_y$ nanowire arrays under Ar and NH_3 atmospheres, respectively (for details, see Experiment). The $Co_x(OH)_y$ precursor was prepared by a modified hydrothermal method (for details, see Experiment).

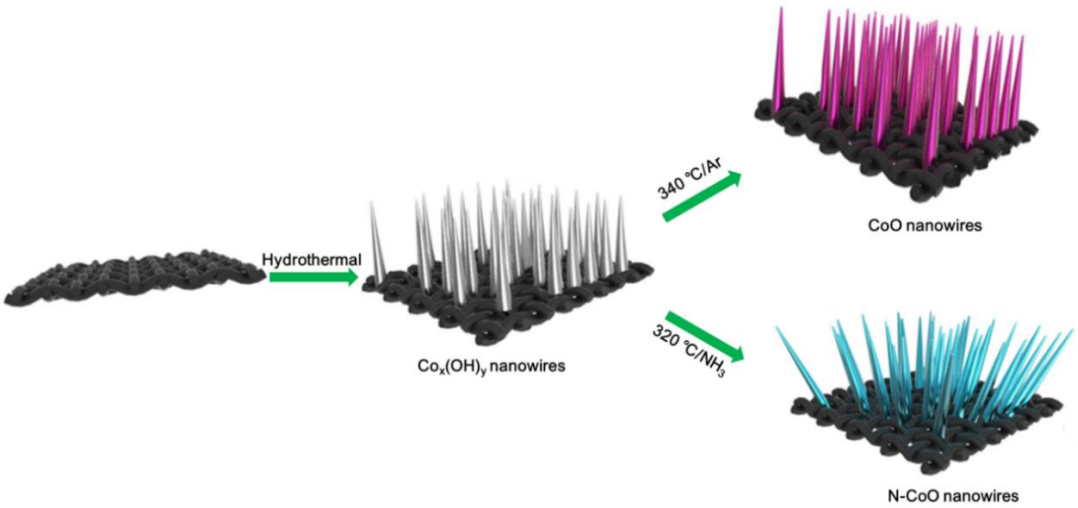

Figure 1. The schematic illustration for the preparation of CoO and N-CoO nanowires.

The N-CoO nanowire arrays were prepared by the topotactical transformation of the pre-synthesized $Co_x(OH)_y$ nanowire arrays using a nitrogen strategy. The XRD patterns of the CoO and N-CoO nanowire arrays in Figure 2a corresponded to the crystal structure of CoO (JCPDS: 01-078-0431), suggesting the precursor of the $Co_x(OH)_y$ nanowire arrays could convert into CoO and N-CoO nanowire arrays after annealing under Ar and NH_3 atmospheres, respectively. The SEM images of Figures 2b and S1 show the morphology of $Co_x(OH)_y$ with dense nanowire arrays on the carbon cloth (CC). The SEM images of CoO and N-CoO in Figure 2c,d display the overall sheet-like morphology of the $Co_x(OH)_y$ nanowire arrays. However, compared to the smooth surface of the CoO nanowire arrays, the surface of the N-CoO nanowire arrays became rough after nitrogen treatment. The TEM image of N-CoO in Figure S2 further demonstrates the morphology and the length of about 1.5 μm. The distribution of Co, O and N elements in N-CoO were determined using energy-dispersive spectroscopy (EDS). The recorded elemental mappings revealed Co, O and N elements were uniformly distributed in N-CoO (Figure 2e). Generally, XRD, SEM, TEM and elemental mappings demonstrated that N atoms were incorporated into a lattice of CoO nanowire arrays.

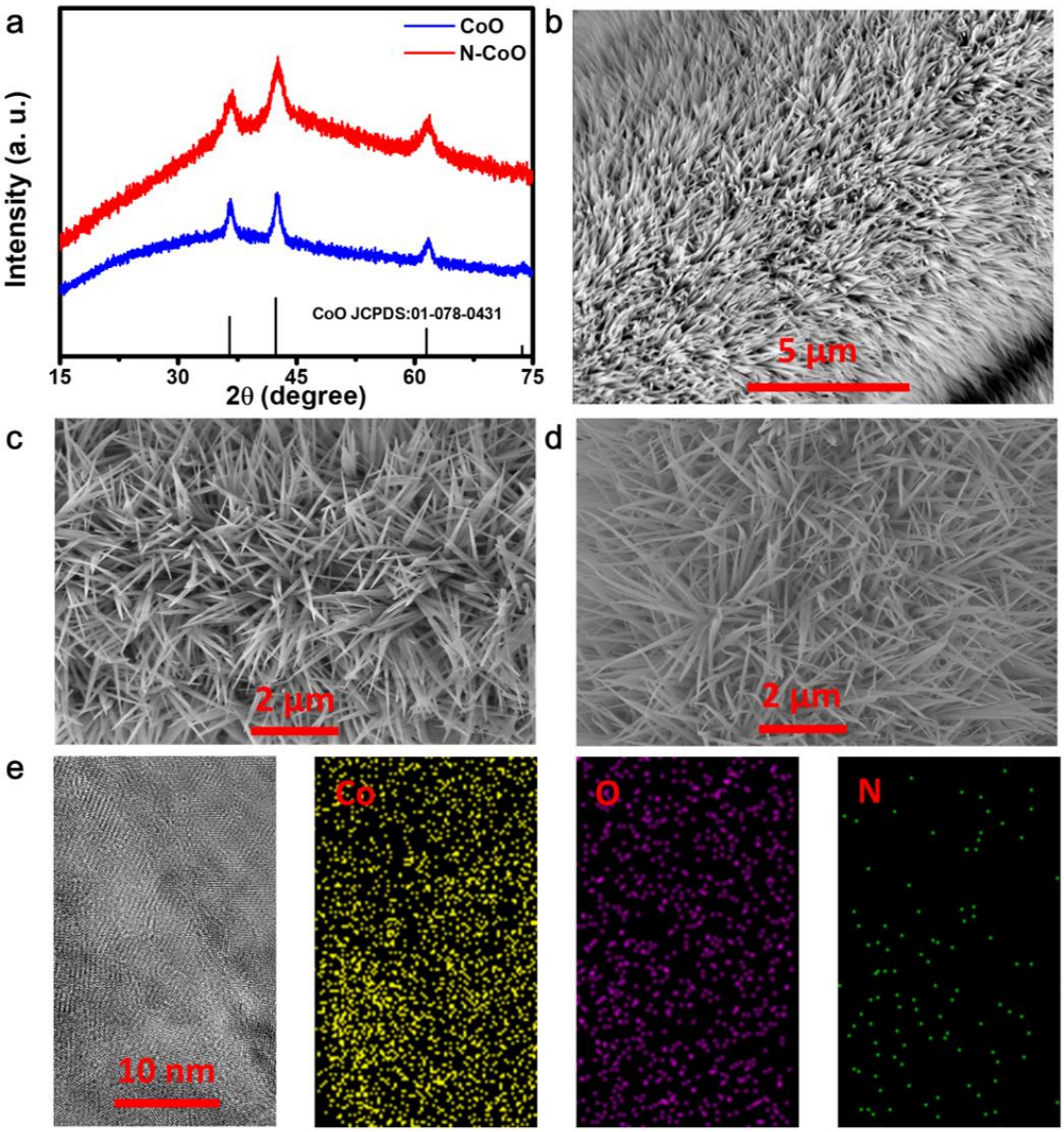

Figure 2. (**a**) XRD patterns of CoO and N-CoO nanowire arrays. (**b**–**d**) SEM images of $Co_x(OH)_y$, CoO and N-CoO nanowire arrays. (**e**) Element mappings of Co, O and N in N-CoO nanowire arrays.

XPS measurements were carried out to study the electronic structure of the surface elements of CoO and N-CoO nanowire arrays. Figure 3a shows the high-resolution XPS spectra of C 1s, which were used as the reference standard (peak at 284.6 eV) for elements of Co, O and N. As seen in Figure 2b, the element peaks of C 1s, O 1s could be clearly seen in the survey scan spectra of the CoO and N-CoO nanowire arrays. However, compared with CoO, there was a weak peak at around 400 eV, suggesting the existence of the N element in N-CoO. Figure 2c depicts the high-resolution XPS spectra of N 1s, further demonstrating the presence of N in N-CoO, which was consistent with the results of the element mappings. Figure 2d shows the high-resolution spectra of Co 2p; the broad peaks around 780.7 and 796.8 eV were regarded as Co $2p_{3/2}$ and Co $2p_{1/2}$ due to the spin-orbit coupling. Furthermore, the peak positions of Co $2p_{3/2}$ and Co $2p_{1/2}$ in N-CoO were higher than those in CoO, suggesting that the N incorporation could effectively tune the electronic structure of Co. Figure 2e, f reveal the O 1s spectra of the CoO and N-CoO nanowire arrays.

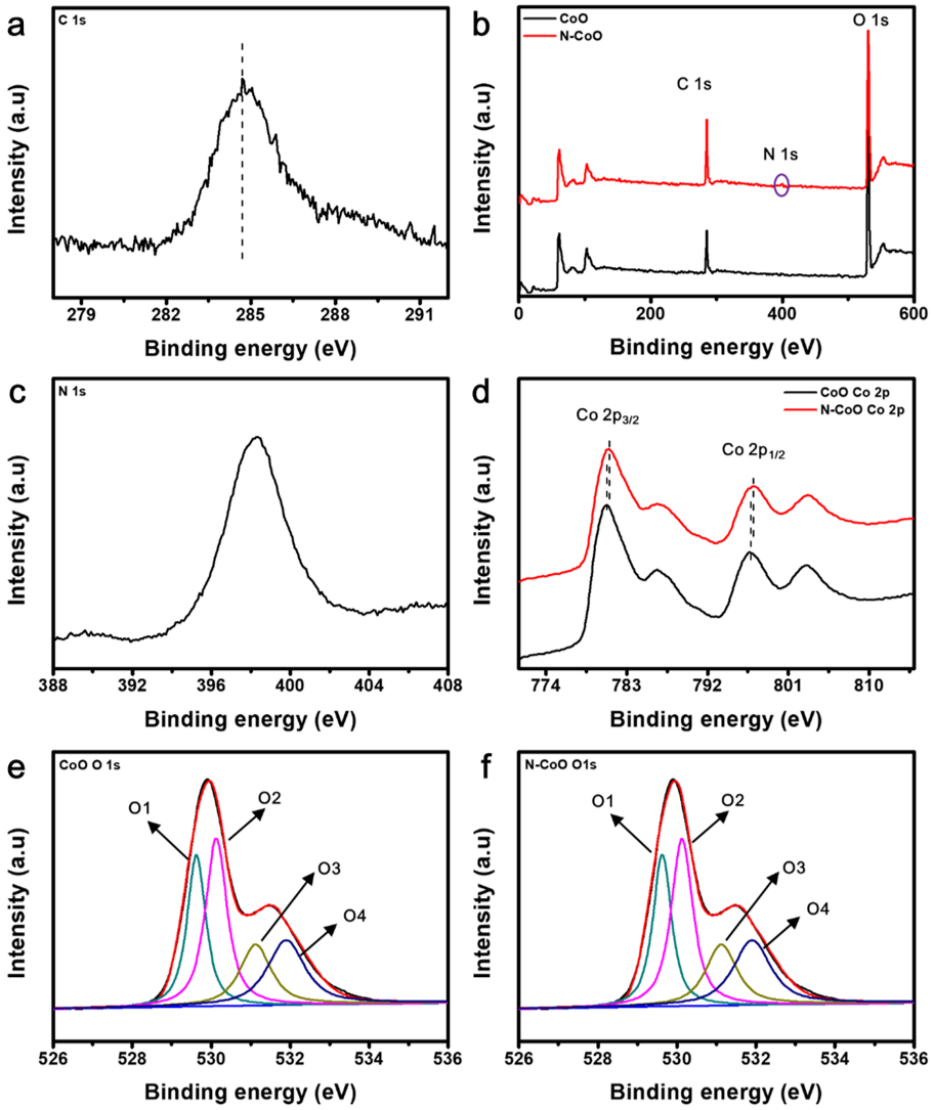

Figure 3. (**a**) High-resolution XPS spectra of C 1s. (**b**) Survey scan spectra of CoO and N-CoO. (**c**) High-resolution XPS spectra of N 1s. (**d**) High-resolution XPS spectra of Co 2p. (**e**) High-resolution XPS spectra of O in CoO. (**f**) High-resolution XPS spectra of O in N-CoO.

S1 displays the percentage of different O constituents. The peak of O1 at approximately 529.6 eV represents the O^{2-} in the crystal lattice of CoO and N-CoO. Compared with the O1 percentage in the CoO nanowire arrays, the percentage of O1 in the N-CoO nanowire arrays

decreased from 26.4% to 22.3%, suggesting the incorporation of N atoms in the lattice of CoO and the formation of oxygen vacancies. The peak of O2 at around 530.1 eV could belong to the OH^-. The variation tendency of O2 was also reduced, indicating that CoO improved the desorption of OH^- after the incorporation of N, which was beneficial for water dissociation in the alkaline solution. The peak of O3 was considered to be adsorbed water molecules on the surfaces of the CoO and N-CoO nanowire arrays. Inversely, the percentage of O3 in N-CoO significantly increased, implying the enhanced capacity of adsorbing water molecules on N-CoO, which was beneficial for the first step of HER in the alkaline solution. The peak of O4 was regarded as oxygen vacancy, which was caused by the reducibility of NH_3 at high temperature. In a word, the XPS analysis indicated that the electronic structure of the CoO nanowire arrays was tuned significantly after introducing N in CoO, which benefitted the HER in the alkaline solution.

Figure 4a displays the LSV curves of the CoO and N-CoO nanowire arrays, with a state-of-the-art Pt/C catalyst as the control sample. Clearly, the N-CoO nanowire arrays displayed a lower onset potential and higher current density than the CoO nanowire arrays, suggesting that the N-CoO nanowire arrays could effectively promote the catalytic activity for HER in the alkaline solution. The overpotential of the N-CoO nanowire arrays at 10 mA cm^{-2} needed only 123 mV, which was apparently much lower than that of CoO (285 mV, Figure 4c). Moreover, the Tafe slope is an important parameter that can reflect the effects of N-doping on HER kinetics. As shown in Figure 4b, the Tafe slope of the CoO nanowire arrays was 160 mV dec^{-1}, suggesting that the Volmer step of water dissociation was the rate-determining step on the catalyst of the CoO nanowire arrays. However, the N-CoO nanowire arrays presented a significantly decreased Tafe slope of 97 mV dec^{-1}, implying the sluggish water dissociation step was accelerated after the incorporation of N in the CoO nanowire arrays. Although the overpotential and Tafe slope of the N-CoO nanowire arrays (123 mV, 97 mV dec^{-1}) were still far from the state-of-the-art Pt/C catalyst (49 mv, 41 mV dec^{-1}), this design strategy provides a simple method to promote water dissociation in alkaline solutions at the atomic level. Further performance improvements of N-CoO nanowire arrays could perhaps include other transition metals in order to better promote water dissociation.

To evaluate the stability of the N-CoO nanowire arrays, long-term stability measurements of chronoamperometric and polarization cycling were performed. As seen in Figure 4d, both of them displayed no obvious decrease, indicating the excellent electrochemical stability of the N-CoO nanowire arrays.

To assess the energy barriers, we studied the effect of temperature on the performance of the CoO and N-CoO nanowire arrays and found the rate constants followed the Arrhenius relationship. The Arrhenius plots for the CoO and N-CoO nanowire arrays allowed us to extract electrochemical activation energies for HER (Figure 5a) [51]. It shows that the N-CoO nanowire arrays exhibited an apparent barrier value of 18.0 kJ mol^{-1}, which was significantly lower than that of CoO (25.9 kJ mol^{-1}). The significantly decreased electrochemical activation energy of N-CoO for HER was consistent with our XPS analysis, which showed that the N-CoO nanowire arrays could boost water dissociation.

To uncover the electro-transfer reaction kinetics, electrochemical impedance spectroscopy (EIS) was measured. Figure 5b displays the Nyquist plots of the CoO and N-CoO nanowire arrays; both of them displayed semi-circles, which could be well-fitted using a simple equivalent circuit composed of electrolyte resistance (Rs), a constant phase element (CPE) and charge-transfer resistance (R_{CT}). The charge-transfer resistance (Rct) of the N-CoO nanowire arrays was calculated to be 38.4 Ω, which was much lower than that of CoO (239.7 Ω), further revealing the much-promoted charge transport kinetics of N-CoO nanowire arrays [52].

Considering the importance of surface area on the HER performance, the electrochemical surface areas of CoO and N-CoO nanowire arrays were obtained from the cyclic voltammograms at the scan rates of 20, 40, 60 and 80 mv s^{-1}. Based on the CVs of Figure S3, the ECSA value of N-CoO was 39.4 mF cm^{-2} (Figure 5c), which was obviously larger than

that of the CoO nanowires (25.5 mF cm^{-2}), suggesting the incorporation of N in CoO improved the number of active sites.

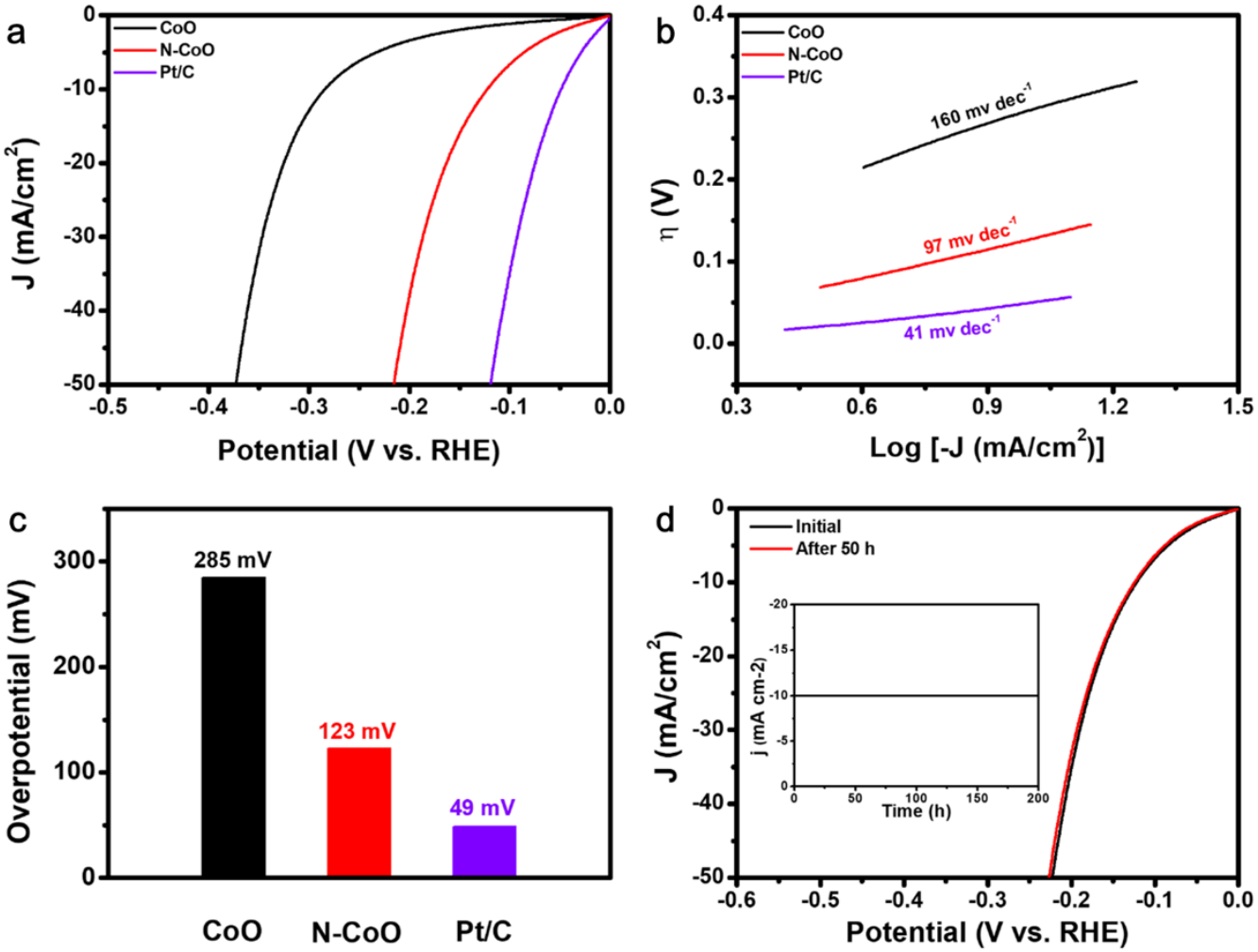

Figure 4. (**a**) LSV curves of the CoO and N-CoO nanowires, with a state-of-the-art Pt/C catalyst as the control sample. (**b**) Tafel slopes of the CoO and N-CoO nanowires, with a state-of-the-art Pt/C catalyst as the control sample. (**c**) The overpotential of the CoO and N-CoO nanowires at a current density of 10 mA cm^{-2}, with a state-of-the-art Pt/C catalyst as the control sample. (**d**) The initial and post-50 h stability tests at 10 mA cm^{-2} LSV curves of the N-CoO nanowires. The inset is the chronoamperometric curve recorded at −0.123 V (10 mA cm^{-2}).

To understand the origin of the high HER performance, the turnover frequency (TOF) of the CoO and N-CoO nanowire arrays was estimated to reveal the intrinsic catalytic activities. The details concerning the obtainment of the TOF values can be found in the supporting information. As shown in Figure 5d, although the surface area of the N-CoO nanowires was obviously larger than that of CoO, the TOF values of the N-CoO nanowires were still significantly larger than that of the CoO nanowires at the same potential, clearly revealing that the incorporation of N in CoO can effectively promote the intrinsic HER activity of N-CoO nanowires [53].

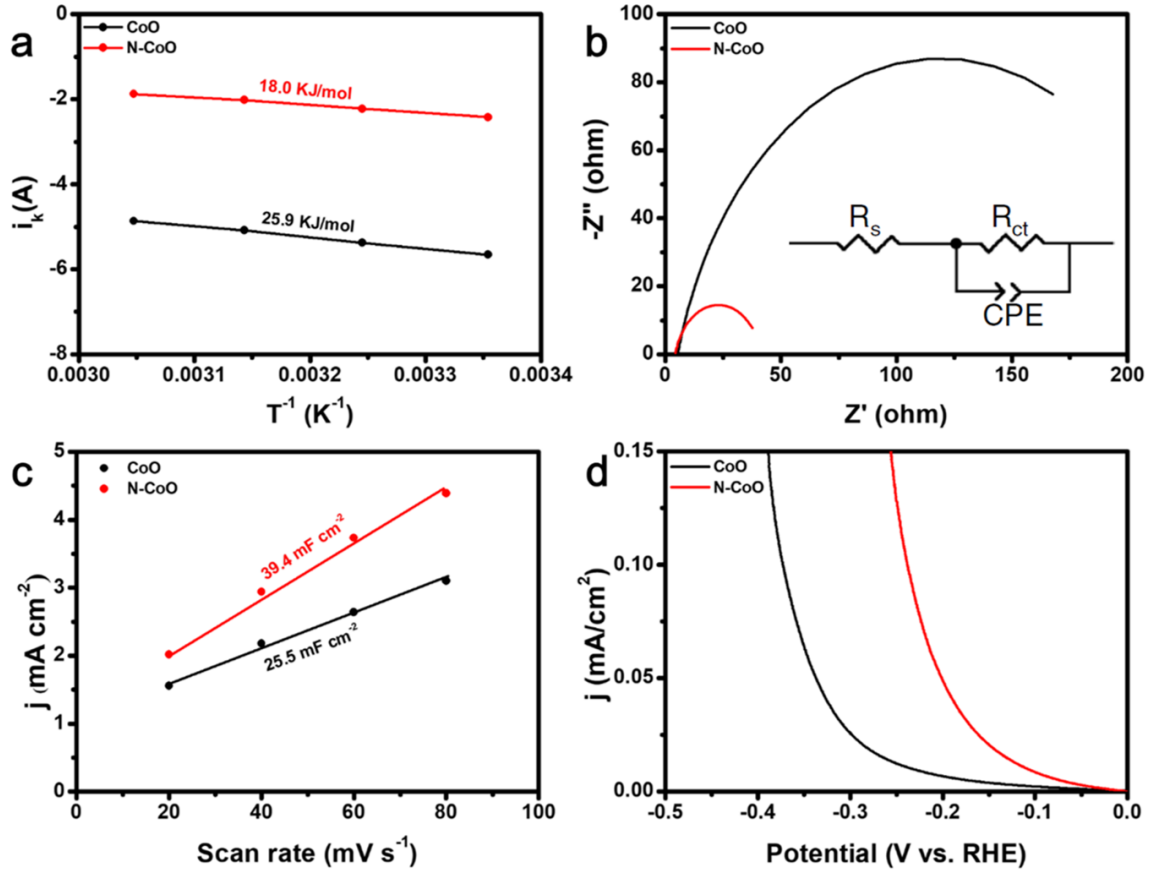

Figure 5. (**a**) Arrhenius plots of the kinetic current at an overpotential of 200 mV for the CoO and N-CoO nanowires. (**b**) EIS of the CoO and N-CoO nanowires. The inset is an equivalent circuit of the CoO and N-CoO nanowires. (**c**) ECSA of the CoO and N-CoO nanowires. (**d**) TOF of the CoO and N-CoO nanowires.

3. Experiment

All of the chemical reagents were analytical grade (AR) and they were all used directly without any further purification. The deionized water (DI) used in all experiments was produced from the water purification apparatus of Milli-Q (18.2 MΩ cm^{-1}). ($Co_2(NO_3)_2{\cdot}6H_2O$), Urea ($H_2C_2O_4$), (NH_4F), (C_3H_6O), and (CH_3CH_2OH) were purchased from Aladdin Reagent Co., LTD. Carbon was purchased from the Taiwan Carbon Energy Co. LTD.

3.1. The Preparation of the CoO and N-CoO Nanowire Arrays

Initially, 40 mmol $Co_2(NO_3)_2{\cdot}6H_2O$, 200 mmol $H_2C_2O_4$ and 80 mmol NH_4F were dissolved in 200 mL deionized water with the help of a magnetic stirring apparatus. Next, a 20 mL solution of the aforementioned mixture and a 2×3 cm^2 CC pretreated with acetone, ethyl alcohol and deionized water were put in a Teflon-lined stainless autoclave. The autoclave was transferred to an oven at 200 °C for 6 h. After the temperature of the autoclave reduced to room temperature, the CC was taken out, cleaned using the deionized water and dried in a vacuum oven at 50 °C for 12 h. Then, the precursor of the $Co_x(OH)_y$ nanowire arrays was prepared by annealing the CC in a muffle furnace at 350 °C for 2 h. Finally, the CoO nanowires were obtained by annealing the Cox(OH)y nanowire arrays at 350 °C in a tube furnace with an argon flow rate of 80 mL/min. The N-CoO nanowire arrays were obtained by annealing the $Co_x(OH)_y$ nanowire arrays at 320 °C in a tube furnace under a NH3 atmosphere with a flow rate of 60 mL/min.

3.2. Materials Characterization

A scanning electron microscope (SEM) and transmission electron microscopy (TEM) were used to obtain the morphology of the $Co_x(OH)_y$, CoO and N-CoO nanowire arrays. XRD was applied to provide the crystal structure of the $Co_x(OH)_y$, CoO and N-CoO nanowire arrays with a Cu Kα as a source (1.54056 Å). An XPS analysis was performed to distinguish the electronic structure of the CoO and N-CoO nanowire arrays.

3.3. Electrochemical Measurements

All the electrochemical tests were performed in 1.0 M KOH with a classic three-electrode system on an IvumStat electrochemical workstation. The CoO and N-CoO nanowire arrays on CC were employed as working electrodes, and the graphite rod and HgO were used as the counter and the reference electrodes, respectively. All the potentials in the work were converted to the values relative to the reversible hydrogen electrode. The linear sweep voltammetry (LSV) curves shown in the work were collected with a scan rate of 2 mv s^{-1}. The stability test for N-CoO nanowire arrays was carried out at the potential of −0.123 V. The overpotential of 50 mV with a perturbation amplitude of 10 mV was performed in the measurements of electrochemical impedance spectroscopy (EIS) in a frequency from 10 kHz to 0.1 Hz. The cyclic voltammograms (CVs) in a range between 0 and 0.1 V were used to estimate the electrochemical surface areas (ECSA) at the scan rates of 20, 40, 60, and 80 mV s^{-1}, respectively. The difference values of current density per square centimeter (cm^2) at 0.05 V vs. RHE were plotted with the scan rates in which the slope was used to measure the ECSA. The TOF values were estimated according to the previous literature [54].

For temperature-dependent measurements, the electrochemical reaction cell with electrodes was put in a water bath. The temperature was first improved to a value above 60 °C, then the current values of the catalyst at temperatures of 55, 45, 35 and 25 °C were recorded with the temperature reducing in the environment in order to decrease error. As we all know, the kinetics of chemical reactions increase with rises in temperature which is the same for HER. The relationship between the chemical rate constant and temperature is roughly proportional to $\exp(-\Delta G/kT)$, where ΔG and k are the activation energy and the Boltzmann constant, respectively. Specifically, the approximate activation energy (Ea) for HER can be defined by the Arrhenius relationship

$$ni_k = -\frac{E_a}{RT} + C \quad (1)$$

where T is the test temperature, ik is the current density at an overpotential of −200 mV and R is the gas equilibrium constant. The Ea for different HER catalysts can be obtained by the slopes of various Arrhenius plots (-R×slope).

4. Conclusions

In general, we have demonstrated that the incorporation of N in CoO nanowires can effectively improve the HER performance in an alkaline solution. Compared with the inert HER activity of CoO nanowires, the obtained N-CoO nanowires obviously exhibited increased HER activity, which needed only 123 mV to achieve the current density of 10 mA cm^{-2}. The XPS of Co 2p and O 1s revealed that the electronic structure of CoO was obviously modulated after the incorporation of N, which improved the adsorption and activity of the water molecule. The energy barriers obtained from the Arrhenius relationship of the current density at different temperatures indicated that the N-CoO nanowires accelerated water dissociation in the alkaline solution. This work provides a new design insight for the development of Pt-free catalysts with a high performance for HER in alkaline solutions at the atomic scale.

Supplementary Materials: The following are available online at https://www.mdpi.com/article/10.3390/catal11101237/s1, Figure S1: SEM image of Cox(OH)y nanowires, Figure S2: TEM image of N-CoO nanowires, Figure S3: ECSA of CoO and N-CoO nanowires, Table S1: The percentage of O1, O2, O3 and O4 in CoO and N-CoO.

Author Contributions: Conceptualization, M.C., H.D. and H.Z.; methodology, M.C.; software, J.L.; validation, M.C., H.D., X.L. and H.Z.; formal analysis, D.W.; investigation, S.S.; resources, M.C.; data curation, D.W., D.X., X.L. and S.S.; writing—original draft preparation, H.D.; writing—review and editing, M.C., H.D. and H.Z.; visualization, H.Z.; supervision, H.Z. All authors have read and agreed to the published version of the manuscript.

Funding: This research was funded by the Education Department of Guizhou Province, grant number [2019]213, [2018]424, [2020]206, QNYSKYPT2018005 and the Science and Technology Department of Guizhou Province, grant number [2020]QNSYXM03.

Data Availability Statement: Not applicable.

Acknowledgments: We acknowledge the Min Liu's group of Central South University for SEM, TEM and XPS characterizations.

Conflicts of Interest: The authors declare no conflict of interest.

References

1. Kalair, A.; Abas, N.; Saleem, M.S.; Kalair, A.R.; Khan, N. Role of energy storage systems in energy transition from fossil fuels to renewables. *Energy Storage* **2021**, *3*, e135. [CrossRef]
2. Anser, M.K.; Hanif, I.; Vo, X.V.; Alharthi, M. The long-run and short-run influence of environmental pollution, energy consumption, and economic activities on health quality in emerging countries. *Environ. Sci. Pollut. Res.* **2020**, *27*, 32518–32532. [CrossRef]
3. Bailis, R.; Ezzati, M.; Kammen Daniel, M. Mortality and Greenhouse Gas Impacts of Biomass and Petroleum energy futures in Africa. *Science* **2005**, *308*, 98–103. [CrossRef]
4. Ghosh, U.; Majumdar, A.; Pal, A. Photocatalytic CO_2 reduction over g-C_3N_4 based heterostructures: Recent progress and prospects. *J. Environ. Chem. Eng.* **2021**, *9*, 104631. [CrossRef]
5. Patel, P.; Patel, B.; Vekaria, E.; Shah, M. Biophysical economics and management of biodiesel, a harbinger of clean and sustainable energy. *Int. J. Energy Water Resour.* **2020**, *4*, 411–423. [CrossRef]
6. Yaqoob, L.; Noor, T.; Iqbal, N. Recent progress in development of efficient electrocatalyst for methanol oxidation reaction in direct methanol fuel cell. *Int. J. Energy Res.* **2021**, *45*, 6550–6583. [CrossRef]
7. Gonçalves, J.M.; Martins, P.R.; Araki, K.; Angnes, L. Recent progress in water splitting and hybrid supercapacitors based on nickel-vanadium layered double hydroxides. *J. Energy Chem.* **2021**, *57*, 496–515. [CrossRef]
8. Cao, M.; Sun, S.; Long, C.; Luo, J.; Wu, D. Microporous metal phosphonate-based N-doped graphene oxide for efficient electrocatalyst for water oxidation. *Mater. Lett.* **2021**, *284*, 128891. [CrossRef]
9. Turner, J.A. Sustainable hydrogen production. *Science* **2004**, *305*, 972–974. [CrossRef]
10. Dinh, C.T.; Jain, A.; Arquer, F.P.G.; De Luna, P.; Li, J.; Wang, N.; Zheng, X.; Cai, J.; Gregory, B.Z.; Voznyy, O.; et al. Multi-site electrocatalysts for hydrogen evolution in neutral media by destabilization of water molecules. *Nat. Energy* **2018**, *4*, 107–114. [CrossRef]
11. You, B.; Liu, X.; Hu, G.; Gul, S.; Yano, J.; Jiang, D.E.; Sun, Y. Universal Surface Engineering of Transition Metals for Superior Electrocatalytic Hydrogen Evolution in Neutral Water. *J. Am. Chem. Soc.* **2017**, *139*, 12283–12290. [CrossRef]
12. Liu, Z.; Li, J.; Zhang, J.; Qin, M.; Yang, G.; Tang, Y. Ultrafine Ir Nanowires with Microporous Channels and Superior Electrocatalytic Activity for Oxygen Evolution Reaction. *ChemCatChem* **2020**, *12*, 3060–3067. [CrossRef]
13. Bizzotto, F.; Quinson, J.; Zana, A.; Dworzak, A.; Arenz, M. Ir nanoparticles with ultrahigh dispersion as oxygen evolution reaction (OER) catalyst: Synthesis and activity benchmarking. *Catal. Sci. Technol.* **2019**, *9*, 6345–6356. [CrossRef]
14. Yin, P.; Wu, G.; Wang, X.; Liu, S.; Zhou, F.; Dai, L.; Wang, X.; Yang, B.; Yu, Z.Q. NiCo-LDH nanosheets strongly coupled with GO-CNTs as a hybrid electrocatalyst for oxygen evolution reaction. *Nano Res.* **2021**, *4*, 1–6. [CrossRef]
15. Pan, S.; Yu, J.; Zhang, Y.; Li, B. Facile and novel strategy to fabricate 2D alpha-$Co(OH)_2$ nanosheets for efficient oxygen evolution reaction application. *Mater. Lett.* **2020**, *278*, 128414. [CrossRef]
16. Yuan, R.; Jiang, M.; Gao, S.; Wang, Z.; Wang, H.; Boczkaj, G.; Liu, Z.; Ma, J.; Li, Z. 3D mesoporous α-$Co(OH)_2$ nanosheets electrodeposited on nickel foam: A new generation of macroscopic cobalt-based hybrid for peroxymonosulfate activation. *Chem. Eng. J.* **2020**, *380*, 122447. [CrossRef]
17. Mahmood, N.; Yao, Y.; Zhang, J.W.; Pan, L.; Zhang, X.; Zou, J.J. Electrocatalysts for Hydrogen Evolution in Alkaline Electrolytes: Mechanisms, Challenges, and Prospective Solutions. *Adv. Sci.* **2018**, *5*, 1700464. [CrossRef] [PubMed]
18. Zhu, Y.P.; Guo, C.; Zheng, Y.; Qiao, S.Z. Surface and Interface Engineering of Noble-Metal-Free Electrocatalysts for Efficient Energy Conversion Processes. *Acc. Chem. Res.* **2017**, *50*, 915–923. [CrossRef]

19. Wang, X.; Zheng, Y.; Sheng, W.; Xu, Z.J.; Jaroniec, M.; Qiao, S.Z. Strategies for design of electrocatalysts for hydrogen evolution under alkaline conditions. *Mater. Today* **2020**, *36*, 125–138. [CrossRef]
20. Chen, J.; Ge, Y.; Feng, Q.; Zhuang, P.; Chu, H.; Cao, Y.; Smith, W.R.; Dong, P.; Ye, M.; Shen, J. Nesting Co_3Mo Binary Alloy Nanoparticles onto Molybdenum Oxide Nanosheet Arrays for Superior Hydrogen Evolution Reaction. *ACS Appl. Mater. Interfaces* **2019**, *11*, 9002–9010. [CrossRef] [PubMed]
21. Nairan, A.; Zou, P.; Liang, C.; Liu, J.; Wu, D.; Liu, P.; Yang, C. NiMo Solid Solution Nanowire Array Electrodes for Highly Efficient Hydrogen Evolution Reaction. *Adv. Funct. Mater.* **2019**, *29*, 1903747. [CrossRef]
22. Yang, L.; Zeng, L.; Liu, H.; Deng, Y.; Zhou, Z.; Yu, J.; Liu, H.; Zhou, W. Hierarchical microsphere of MoNi porous nanosheets as electrocatalyst and cocatalyst for hydrogen evolution reaction. *Appl. Catal. B Environ.* **2019**, *249*, 98–105. [CrossRef]
23. Xia, M.; Lei, T.; Lv, N.; Li, N. Synthesis and electrocatalytic hydrogen evolution performance of Ni–Mo–Cu alloy coating electrode. *Int. J. Hydrogen Energy* **2014**, *39*, 4794–4802. [CrossRef]
24. Zhang, J.; Wang, T.; Liu, P.; Liao, Z.; Liu, S.; Zhuang, X.; Chen, M.; Zschech, E.; Feng, X. Efficient hydrogen production on $MoNi_4$ electrocatalysts with fast water dissociation kinetics. *Nat. Commun.* **2017**, *8*, 15437. [CrossRef]
25. Chen, Z.; Song, Y.; Cai, J.; Zheng, X.; Han, D.; Wu, Y.; Zang, Y.; Niu, S.; Liu, Y.; Zhu, J.; et al. Tailoring the d-Band Centers Enables Co_4N Nanosheets To Be Highly Active for Hydrogen Evolution Catalysis. *Angew. Chem. Int. Ed. Engl.* **2018**, *57*, 5076–5080. [CrossRef]
26. Lei, C.; Wang, Y.; Hou, Y.; Liu, P.; Yang, J.; Zhang, T.; Zhuang, X.; Chen, M.; Yang, B.; Lei, L.; et al. Efficient alkaline hydrogen evolution on atomically dispersed Ni–N_x Species anchored porous carbon with embedded Ni nanoparticles by accelerating water dissociation kinetics. *Energy Environ. Sci.* **2019**, *12*, 149–156. [CrossRef]
27. Harnisch, F.; Sievers, G.; Schröder, U. Tungsten carbide as electrocatalyst for the hydrogen evolution reaction in pH neutral electrolyte solutions. *Appl. Catal. B Environ.* **2009**, *89*, 455–458. [CrossRef]
28. Shi, J.; Pu, Z.; Liu, Q.; Asiri, A.M.; Hu, J.; Sun, X. Tungsten nitride nanorods array grown on carbon cloth as an efficient hydrogen evolution cathode at all pH values. *Electrochim. Acta* **2015**, *154*, 345–351. [CrossRef]
29. Miao, M.; Pan, J.; He, T.; Yan, Y.; Xia, B.Y.; Wang, X. Molybdenum Carbide-Based Electrocatalysts for Hydrogen Evolution Reaction. *Chem. A Eur. J.* **2017**, *23*, 10947–10961. [CrossRef] [PubMed]
30. Men, Y.; Li, P.; Zhou, J.; Cheng, G.; Chen, S.; Luo, W. Tailoring the Electronic Structure of Co_2P by N Doping for Boosting Hydrogen Evolution Reaction at All pH Values. *ACS Catal.* **2019**, *9*, 3744–3752. [CrossRef]
31. He, Q.; Tian, D.; Jiang, H.; Cao, D.; Wei, S.; Liu, D.; Song, P.; Lin, Y.; Song, L. Achieving Efficient Alkaline Hydrogen Evolution Reaction over a Ni_5P_4 Catalyst Incorporating Single-Atomic Ru Sites. *Adv. Mater.* **2020**, *32*, e1906972. [CrossRef] [PubMed]
32. Yang, G.; Jiao, Y.; Yan, H.; Xie, Y.; Wu, A.; Dong, X.; Guo, D.; Tian, C.; Fu, H. Interfacial Engineering of MoO_2-FeP Heterojunction for Highly Efficient Hydrogen Evolution Coupled with Biomass Electrooxidation. *Adv. Mater.* **2020**, *32*, e2000455. [CrossRef] [PubMed]
33. Li, Y.; Wang, H.; Xie, L.; Liang, Y.; Hong, G.; Dai, H. MoS_2 Nanoparticles Grown on Graphene: An Advanced Catalyst for the Hydrogen Evolution Reaction. *J. Am. Chem. Soc.* **2011**, *133*, 7296–7299. [CrossRef]
34. Voiry, D.; Salehi, M.; Silva, R.; Fujita, T.; Chen, M.; Asefa, T.; Shenoy, V.; Eda, G.; Chhowalla, M. Conducting MoS_2 Nanosheets as Catalysts for Hydrogen Evolution Reaction. *Nano Lett.* **2013**, *13*, 6222–6227. [CrossRef]
35. Cheng, L.; Huang, W.; Gong, Q.; Liu, C.; Liu, Z.; Li, Y.; Dai, H. Ultrathin WS2 Nanoflakes as a High-Performance Electrocatalyst for the Hydrogen Evolution Reaction. *Angew. Chem. Int. Ed.* **2014**, *53*, 7860–7863. [CrossRef]
36. Frank, A.J.; Honda, K. Polymer-modified electrodes, catalysis and water-splitting reactions. *J. Photochem.* **1985**, *29*, 195–204. [CrossRef]
37. Lahiri, A.; Li, G.; Endres, F. Highly efficient electrocatalytic hydrogen evolution reaction on carbonized porous conducting polymers. *J. Solid State Electrochem.* **2020**, *24*, 2763–2771. [CrossRef]
38. Elias, X.; Liu, Q.; Gimbert-Suriñach, C.; Matheu, R.; Mantilla-Perez, P.; Martinez-Otero, A.; Sala, X.; Martorell, J.; Llobet, A. Neutral water splitting catalysis with a high ff triple junction polymer cell. *ACS Catal.* **2016**, *6*, 3310–3316. [CrossRef]
39. Wang, L.; Zhang, Y.; Chen, L.; Xu, H.; Xiong, Y. 2d polymers as emerging materials for photocatalytic overall water splitting. *Adv. Mater.* **2018**, *30*, 1801955. [CrossRef]
40. Lahiri, A.; Chutia, A.; Carstens, T.; Endres, F. Surface-oxygen induced electrochemical self-assembly of mesoporous conducting polymers for electrocatalysis. *J. Electrochem. Soc.* **2020**, *167*, 112501. [CrossRef]
41. Subbaraman, R.; Tripkovic, D.; Strmcnik, D.; Chang, K.-C.; Uchimura, M.; Paulikas, A.P.; Stamenkovic, V.; Markovic, N.M. Enhancing Hydrogen Evolution Activity in Water Splitting by Tailoring Li^+-$Ni(OH)_2$-Pt Interfaces. *Science* **2011**, *334*, 1256–1260. [CrossRef]
42. Wu, Y.; Liu, X.; Han, D.; Song, X.; Shi, L.; Song, Y.; Niu, S.; Xie, Y.; Cai, J.; Wu, S.; et al. Electron density modulation of $NiCo_2S_4$ nanowires by nitrogen incorporation for highly efficient hydrogen evolution catalysis. *Nat. Commun.* **2018**, *9*, 1425. [CrossRef]
43. Liu, X.; Ni, K.; Niu, C.; Guo, R.; Xi, W.; Wang, Z.; Meng, J.; Li, J.; Zhu, Y.; Wu, P.; et al. Upraising the O 2p Orbital by Integrating Ni with MoO_2 for Accelerating Hydrogen Evolution Kinetics. *ACS Catal.* **2019**, *9*, 2275–2285. [CrossRef]
44. Danilovic, N.; Subbaraman, R.; Strmcnik, D.; Chang, K.C.; Paulikas, A.P.; Stamenkovic, V.R.; Markovic, N.M. Enhancing the Alkaline Hydrogen Evolution Reaction Activity through the Bifunctionality of $Ni(OH)_2$/Metal Catalysts. *Angew. Chem. Int. Ed.* **2012**, *51*, 12495–12498. [CrossRef]

45. Wang, Y.; Chen, L.; Yu, X.; Wang, Y.; Zheng, G. Superb Alkaline Hydrogen Evolution and Simultaneous Electricity Generation by Pt-Decorated Ni_3N Nanosheets. *Adv. Energy Mater.* **2017**, *7*, 1601390. [CrossRef]
46. Lao, M.; Rui, K.; Zhao, G.; Cui, P.; Zheng, X.; Dou, S.X.; Sun, W. Platinum/Nickel Bicarbonate Heterostructures towards Accelerated Hydrogen Evolution under Alkaline Conditions. *Angew. Chem. Int. Ed. Engl.* **2019**, *58*, 5432–5437. [CrossRef]
47. Zhang, J.; Wang, T.; Liu, P.; Liu, S.; Dong, R.; Zhuang, X.; Chen, M.; Feng, X. Engineering water dissociation sites in MoS_2 nanosheets for accelerated electrocatalytic hydrogen production. *Energy Environ. Sci.* **2016**, *9*, 2789–2793. [CrossRef]
48. Zhou, G.; Li, M.; Li, Y.; Dong, H.; Sun, D.; Liu, X.; Xu, L.; Tian, Z.; Tang, Y. Regulating the Electronic Structure of CoP Nanosheets by O Incorporation for High-Efficiency Electrochemical Overall Water Splitting. *Adv. Funct. Mater.* **2019**, *30*, 1905252. [CrossRef]
49. Xu, K.; Ding, H.; Zhang, M.; Chen, M.; Hao, Z.; Zhang, L.; Wu, C.; Xie, Y. Regulating Water-Reduction Kinetics in Cobalt Phosphide for Enhancing HER Catalytic Activity in Alkaline Solution. *Adv. Mater.* **2017**, *29*, 1606980. [CrossRef] [PubMed]
50. Ling, T.; Yan, D.Y.; Wang, H.; Jiao, Y.; Hu, Z.; Zheng, Y.; Zheng, L.; Mao, J.; Liu, H.; Du, X.W.; et al. Activating cobalt(II) oxide nanorods for efficient electrocatalysis by strain engineering. *Nat. Commun.* **2017**, *8*, 1509. [CrossRef] [PubMed]
51. Zhang, B.; Zheng, X.; Voznyy, O.; Comin, R.; Bajdich, M.; García-Melchor, M.; Han, L.; Xu, J.; Liu, M.; Zheng, L.; et al. Homogeneously dispersed multimetal oxygen-evolving catalysts. *Science* **2016**, *352*, 333. [CrossRef] [PubMed]
52. Xie, Y.; Cai, J.; Wu, Y.; Zang, Y.; Zheng, X.; Ye, J.; Cui, P.; Niu, S.; Liu, Y.; Zhu, J.; et al. Boosting Water Dissociation Kinetics on Pt-Ni Nanowires by N-Induced Orbital Tuning. *Adv. Mater.* **2019**, *31*, e1807780. [CrossRef] [PubMed]
53. Zang, Y.; Niu, S.; Wu, Y.; Zheng, X.; Cai, J.; Ye, J.; Xie, Y.; Liu, Y.; Zhou, J.; Zhu, J.; et al. Tuning orbital orientation endows molybdenum disulfide with exceptional alkaline hydrogen evolution capability. *Nat. Commun.* **2019**, *10*, 1217. [CrossRef] [PubMed]
54. Kibsgaard, J.; Jaramillo, T.F. Molybdenum Phosphosulfide: An Active, Acid-Stable, Earth-Abundant Catalyst for the Hydrogen Evolution Reaction. *Angew. Chem. Int. Ed.* **2014**, *53*, 14433–14437. [CrossRef] [PubMed]